Available online at www.sciencedirect.com
ScienceDirect
Journal of Computational Physics 227 (2008) 6720–6726
JOURNAL OF COMPUTATIONAL PHYSICS
www.elsevier.com/locate/jcp

Short Note

Nanoscale adaptive meshing for rapid STM imaging

Stéphane Bedwani [a,*], François Guibault [b], Alain Rochefort [a,*]

[a] Department of Engineering Physics and Regroupement québécois sur les matériaux de pointe (RQMP), École Polytechnique de Montréal, C.P. 6079, Succ. Centre-ville, Montréal, Québec, Canada H3C 3A7
[b] Department of Computer Engineering, École Polytechnique de Montréal, Montréal, Québec, Canada H3C 3A7

Received 31 March 2008; accepted 1 April 2008
Available online 15 April 2008

PACS: 07.05.Tp; 73.40.Gk; 02.60.Gf; 05.60.Gg

Keywords: Mesh adaptation; Scanning tunneling microscopy (STM); Delaunay triangulation; Computational imaging

1. Introduction

The numerical evaluation of individual tunnel currents (pixels) constitutes the bottleneck of fast scanning tunneling microscopy (STM) imaging. The number and the position of grid points where the current is punctually evaluated have to be judiciously chosen to reveal the most important contrasts. In this note, we present an adaptive meshing approach that significantly accelerates the computation time to produce STM images by reducing the number of pixels to evaluate without affecting the final image resolution. This method iteratively reveals the STM image by selecting new probing locations that improves the image quality at each step.

A straightforward method to compute a STM image is to send a high resolution square grid to a solver that will return a pixel color intensity for each node [1,2]. Since pixel calculation is the most time consuming step but is independent of the grid quality, redefining the surface discretization will reduce the amount of computed pixels and thus the time required to compute an image. This process is a step by step image analysis in which zones of interest, such as contrasts related to adsorbed molecules or structural defects, are identified. Contrarily to mesh modeling where one creates an optimized mesh from a high resolution solution, here we want to iteratively build an optimized mesh from a coarse and previous solution. A Delaunay triangulation has been used to efficiently generate optimized meshes from high resolution images [3], and a similar discretization scheme is used in the present work. During mesh generation, standard point insertion algorithms [4] are favored over methods that enable coarsening and smoothing operations [5], since displacing or removing already computed pixels will results in undesirable exclusion of already computed data.

* Corresponding authors. Tel./fax: +1 514 340 4711 (A. Rochefort).
E-mail addresses: stephane.bedwani@polymtl.ca (S. Bedwani), francois.guibault@polymtl.ca (F. Guibault), alain.rochefort@polymtl.ca (A. Rochefort).

doi:10.1016/j.jcp.2008.04.005

2. Methodology

Simulated STM images have particular characteristics that need to be considered while meshing. First, they are essentially made of smooth contrasts, i.e. the solution is noiseless and has no strong discontinuities. This allows efficient image analysis while using a first and second order differentiation approach of intensities. Second, the tunnel current calculation is independent of the surface location. This means that several currents can be computed at the same time on a parallel computer, and the current locations can be non-uniform.

The main steps of our adaptive algorithm are presented as follows. First, the surface of a molecular system is discretized using an initial unstructured mesh. Mesh construction uses a Delaunay triangulation, which is an efficient and well known meshing technique that can be easily implemented. The first adaptive cycle begins by computing a tunneling current at each node of the initial mesh. Then, the computed image intensities are rendered and analyzed to detect the edges from image contrast. Once the edge detection is complete, weights are assigned to the triangles to determine which ones need to be refined at their barycenter to improve image resolution. A new adaptive refinement cycle begins by computing the tunneling current at each new node of the mesh followed by another image analysis. The surface analysis and solving process is repeated until the target resolution is obtained. These image analysis steps of the adaptive algorithms represent less than 1% of the time consumed to evaluate a single pixel.

2.1. Initial mesh

As a first step before adaptation, an initial mesh must present the following characteristics to obtain an accurate adapted solution. First, mesh points must be distributed uniformly across the surface to prevent small contrasts from being ignored during the image analysis step. Second, mesh density can be increased in areas more susceptible to contain contrasts. An STM image is based on the electronic properties of the surface atoms rather then their position, but, while studying a molecular system, it is reasonable to put an emphasis on locations near the studied molecules. The initial resolution may also be significantly coarser then the final image resolution, which usually corresponds to the highest resolutions obtained experimentally ($\sim$0.2 Å). If the initial mesh is too coarse, the image analysis will omit to detect some areas of interest and the final solution will prove incomplete. A minimal mesh resolution is thus used, that is determined heuristically, based on a priori knowledge of typical feature sizes that must be detected.

2.2. Mesh analysis

On a continuous image, an important variation of the pixel intensities reveals the contrast locations by detecting its edges. On a typical grid image, a differential analysis is usually performed by applying bidimensional discrete differentiation operators. In image processing, these operators are represented by convolution masks applied on an image resulting in edges enhancement; Sobel and Prewitt filters are examples of a gradient operator. In our work, such operators cannot be directly applied on unstructured meshes since they only work on regular grids. Instead, we will approximate these operators using a quadratic regression method [6].

2.2.1. Quadratic fit (QF)

A nodal analysis of an unstructured mesh is possible by quadratically reconstructing a local function using QF over a patch, spanning a subregion of the mesh built as follows. First, a central node and all its surrounding nodes forming a ring of elements is added to the patch. Then, a second ring composed of the nearest elements surrounding the first ring is also included. Applying a least square regression on pixel intensities of a quadratic surface z

$$z(x,y) = a + bx + cy + dx^2 + exy + fy^2 \tag{1}$$

with constant coefficients a, b, c, d, e and f, over a patch of sampling points. These coefficients are obtained by minimizing a residual for a patch of n elements. The regression is optimal if the sampling points are uniformly distributed around the studied node, but remains precise even for skewed elements. During an adaptive cycle, a differential analysis is performed for each mesh point associated to a patch and its fitted surface.

2.2.2. Laplacian operator

A scalar Laplacian operator gives the linear second derivative of the surface z in directions x and y, which is invariant to rotation, and hence is not affected by edges direction. Applying this operator on the quadratic surface approximates the Laplacian for a mesh point h

$$|\mathscr{L}z_h(x,y)| \simeq |2d + 2f|. \tag{2}$$

This operator usually highlights discontinuities of an image, such as dots, lines and edges while ignoring flat surfaces.

2.2.3. Gradient operator

A bidirectional gradient operator over the x- and y-axis can also be used to detect discontinuities independently of their directions by considering the magnitude of the gradient. By applying this operator to a quadratic surface related to a reconstruction of current on a patch centered at node h, the gradient magnitude is approximated by

$$\|\nabla z_h(x,y)\| \simeq \sqrt{(b + 2dx_h + ey_h)^2 + (c + 2fy_h + ex_h)^2}. \tag{3}$$

Both operators presented above are frequently used as edge detectors in image processing, but they do not exactly emphasize the same contrast areas. The Laplacian operator detects curvature variations. In contrast, high gradient magnitudes are related to triangles spanning a region containing sharp edges, and low values indicate flat surfaces.

2.2.4. Contrast detection

According to the nature of the information that needs to be emphasized, mesh refinement is performed on different edge sections identified as inflection areas or slope areas. High Laplacian values indicate inflection areas while high gradient magnitudes are related to slope areas. The *shape detection* (curvature-based) scheme increases the mesh density in the inflection areas and reduces it in slope areas. This can be useful to localize boundaries of a phenomenon under study. In an STM application, this scheme provides information on the maximum interaction range between the molecule and surface. The *high intensity detection* (gradient-based) scheme refines any edge area containing high pixel values and avoids the refinement of low values. This second detection approach will predominantly be used for the STM application, since high tunnel currents usually provide insight into the electronic properties of the adsorbed molecule.

2.3. Pixel calculation

The adaptive mesher is independent of the solver type, if the produced images respect the noiseless and smoothness conditions described previously. Two different solvers have been tested to validate the accuracy of the mesher: a Gaussian solver (GS) and a real STM solver.

The GS is a simple mathematical solver that centers a Gaussian surface on top of each molecular atom found on the scanned surface, where the standard deviation and amplitude depends on the atom nature. The pixel intensity $z(\mathbf{x})$ of a point on the scanned surface is given by the summation of each Gaussian surface at that point. For a planar molecule, the image solution can be associated to its van der Waals surface representation.

The second solver is a rigorous computational approach that exploits Green's-function technique [7] within the Landauer–Büttiker (LB) formalism [8] of tunneling in conjunction with a tight-binding Hamiltonian [9]. The tunnel current I between the tip t and the surface s electrodes is defined by

$$I = \frac{2e}{h}\int_{E_F}^{E_F+eV} \overline{T}_{s\to t}(E)[f_s(E) - f_t(E)]\mathrm{d}E, \tag{4}$$

where e is the electron charge, h is Planck's constant, E_F is the Fermi energy, V is the applied voltage, f_s and f_t are, respectively, the Fermi distribution function of the surface and the tip for a given energy E. $\overline{T}_{s\to t}$ is the transmission function (or transmittance) which represents the summation of transmission probabilities over all conduction channels in the conductor. The electrode t is characterized by an apex a of a few atoms, while

the top layer of the electrode s is represented by an appropriate reconstructed r surface. The transmittance $\overline{T}_{s\to t}$ can be evaluated using a surface Green-function matching method [10]

$$\overline{T}_{s\to t} = \mathrm{Tr}[\Gamma_s G_{ra} \Gamma_t G_{ar}], \tag{5}$$

where $\Gamma_s(\Gamma_t)$ is a matrix describing the interaction between the electrode $s(t)$ and the reconstructed surface (apex) $r(a)$, and G_{ra} and G_{ar} are, respectively, the retarded and advanced Green's-functions describing the charge propagation between r and a, i.e. the tunneling region [9]. It must be emphasized that the evaluation of the tunnel current does not depend on the quality of the grid, and that the quality of the final STM image strictly depends on the choice of individual spatial locations where the current is evaluated.

3. Validation

3.1. Image comparison

The quality of the adapted solution can be verified by comparing the images in Tiff format generated on unstructured meshes with the one obtained on a high resolution uniform grid. From this grid, an exact solution is obtained if the grid resolution is equivalent to the one of the final adapted mesh. To compare two images of size $M \times N$, a high resolution reference solution $z_{\mathrm{ref}}(\mathbf{x})$ with an adapted solution $z_{\mathrm{opt}}(\mathbf{x})$, a pixel by pixel analysis is performed. A common way to evaluate the image compression quality uses the peak signal-to-noise ratio (PSNR) and expresses the value in a logarithmic decibel scale. This method can also be applied to check the quality of the adapted solution over the reference solution

$$\mathrm{PSNR} \equiv 20 \log \left(I_{\max} / \sqrt{\| z_{\mathrm{ref}}(\mathbf{x}) - z_{\mathrm{opt}}(\mathbf{x}) \|^2 / (M \times N)} \right) \mathrm{d}B, \tag{6}$$

where $I_{\max}$ is the maximum value a pixel can reach. In our case, using an 8 bit representation, $I_{\max}$ will be equal to 255. Higher a PSNR value is, more accurate the adapted solution will be.

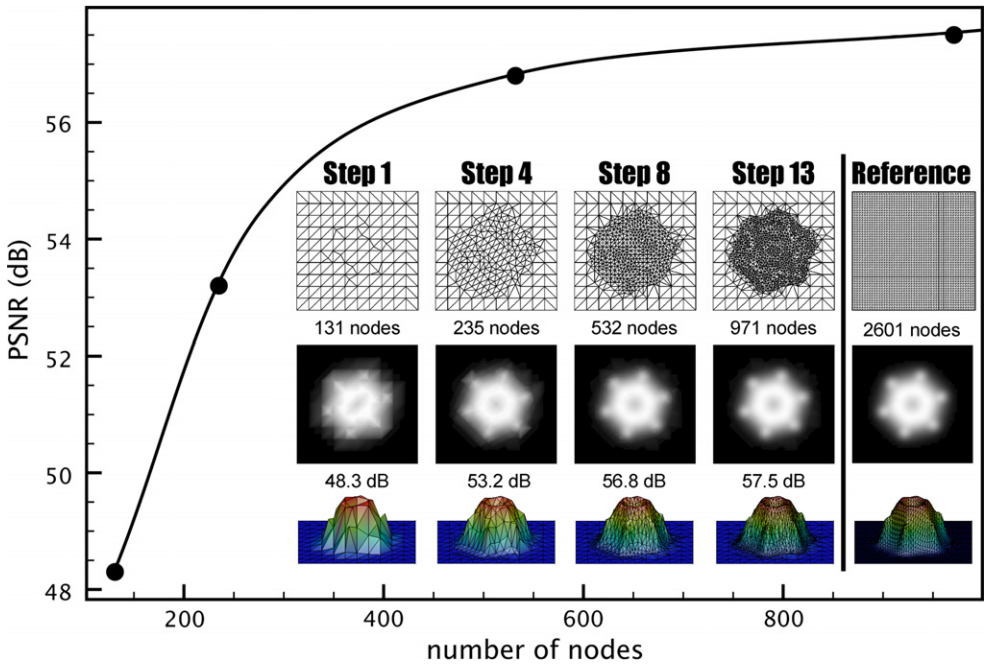

Fig. 1. The main figure shows the variation of the image quality with the number of nodes in the adapted mesh. The inset shows the adapted mesh, and two views of a partial rendering performed after each adaptive cycle. The image solution is obtained from the Gaussian solver using a benzene molecule as an input system. Step 1 shows the initial mesh made from a 1 Å resolution grid. The scanning domain is a (10×10) Å^2 area, and the reference image has 0.2 Å resolution (2601 nodes).

3.2. Partial rendering

By combining an iterative mesh construction with a technique for successive refinement, the STM image can progressively be revealed as the simulation runs. This partial rendering is presented in the inset of Fig. 1 through a series of intermediate meshes obtained at the end of four different adaptive steps, for which two different views of their corresponding image solution are shown. Although the monochrome 2D images basically contains all the intensity features near maxima, only the colored 3D representation can give a clear view of the fine intensity structure related to the atomic nature of the adsorbed benzene molecule. The simulated image is obtained using the Gaussian solver for a benzene molecule adsorbed on a metallic surface. Step 1 shows that quickly, a first low quality image (PSNR = 48.3 dB) is rendered after solving for 131 nodes on the initial mesh. Although this image solution is rough, it supplies enough information for an accurate differential analysis that leads to the new mesh node locations. Each subsequent step increases mesh density in specific areas which improves the image solution quality. Further analysis of the dataset shows that at Step 8, the mesh provides a very accurate image solution (PSNR = 56.8 dB) after solving only 532 tunnel currents. As revealed by the main curve of Fig. 1, we clearly see that good quality images can be obtained even after a few initial mesh adaptation steps.

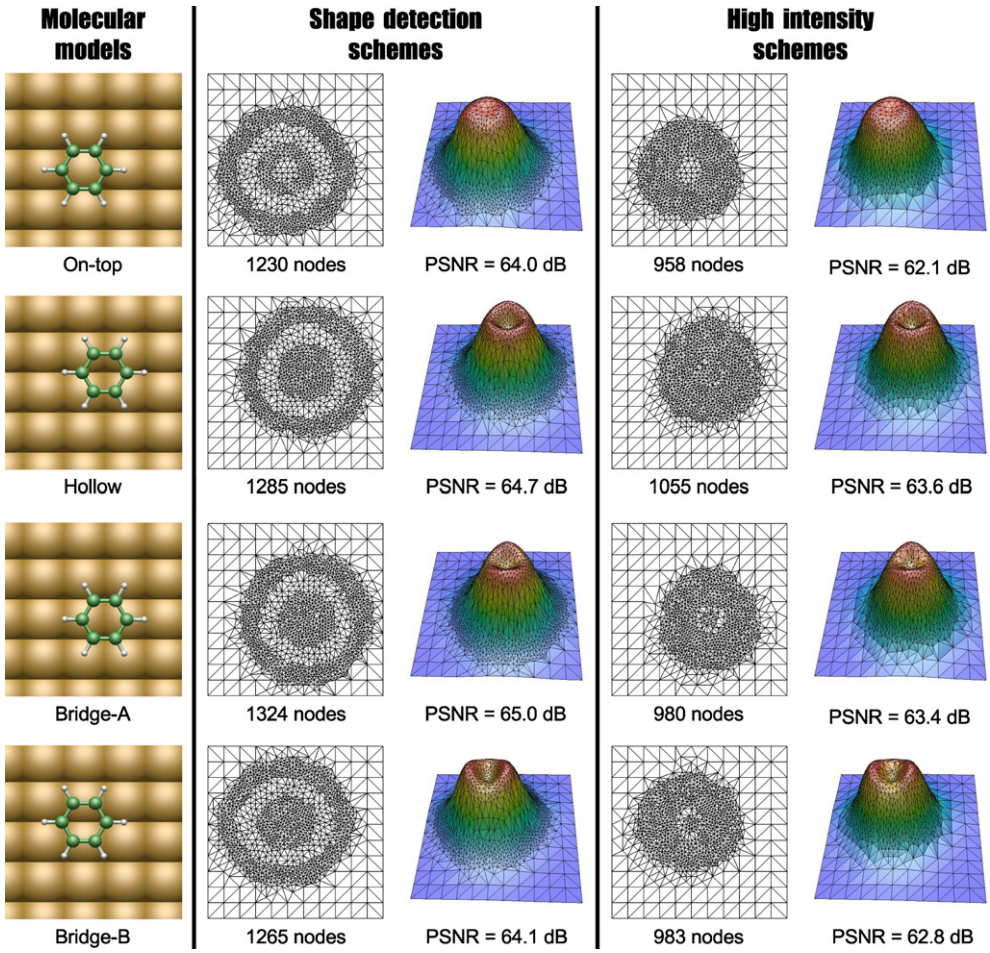

Fig. 2. Simulated STM images of benzene on different adsorption sites of copper (100). Each row shows the input molecular system, followed by the optimized mesh and its STM image for a shape detection scheme and a high intensity scheme. Imaging is done in constant-height mode (5 Å), with a bias voltage of −0.5 V applied between the surface and the W(111) tip. The scanning domain is a 11 × 11 Å square area, and the image comparison was done using a reference image of 0.2 Å resolution (3136 nodes).

4. Results

The STM image of a molecular system may depend on several physical aspects such as the adsorption site. The emblematic example of such site dependance is the adsorption of benzene on Pt(1 1 1) [11,12]. In this section, we explore the adsorption of benzene on a low reactive metal surface such as the Cu(1 0 0). First, this demonstrates how our iterative approach of surface discretization can efficiently adapt to complex STM contrasts. Second, it also provides an accurate representation of high resolution STM images that can be compared to the excellent STM images obtained by Weiss and Eigler on the Pt(1 1 1) surface [11], but also to other surfaces. In our model, both surface and tip electrodes are made of copper (1 0 0), the tip is made of an apex of 10 tungsten atoms. As illustrated in Fig. 2, four adsorption sites were studied: on-top, hollow and two different bridge sites. The constant-height STM images were generated with an applied bias voltage of -0.5 V on a 11×11 Å scanning domain defined by an initial mesh of 155 nodes. In order to avoid any spurious meshing adaptation events, the final images were systematically compared and validated using a high resolution image obtained with a standard square fine grid.

4.1. Adapted STM images

Each molecular system resulted into distinct STM images, and both discretization schemes successfully managed to locate and highlight specific contrast regions while avoiding others. For example, the brightest area of the on-top STM image features a plateau shape involving low first and second order derivatives. Hence, such a flat contrast does not need high resolution, and both proposed discretization schemes avoided to maximize the mesh density in that region. As for the image solution quality, the shape detection scheme obtained better PSNR values ranging from 64.0 to 65.0 dB, compared to the 62.1 to 63.6 dB for the high intensity scheme. However, the high intensity scheme shows greater reduction of the total amount of computed tunnel currents with diminutions ranging from 66.4% to 69.5%, compared to the shape detection scheme which ranges between 57.8% and 60.7%. Finally, the colored 3D representation remains the most accurate approach to reveal the fine atomic structures near maximal intensities which are clearly related to the symmetry of the adsorption site.

This adsorption site dependance found on Cu(1 0 0) is consistent with previous experimental and theoretical works. One particular experimental STM study [13] on Cu(1 0 0) has shown an STM image with a protrusion-like feature that is very similar to the one obtained for an on-top site. Subsequent theoretical study has provided some explanations of STM contrasts using simulated STM images based on the Tersoff–Hamann (TH) model [14] for on-top, bridge-A and hollow adsorption sites of Cu(1 0 0) [15]. Our STM results based on the LB formalism are in agreement with their theoretical interpretation of STM images. Their on-top image shows also a high symmetry, and their bridge-A image is elongated along the same axis as our protrusion splitting. Although this protrusion splitting was not observed within TH limits, a similar feature was observed in a more recent theoretical study of benzene adsorbed on a Cu(1 1 0) surface [16].

5. Conclusion

We have demonstrated a novel approach for space discretization in STM imaging. This technique starts from a simple but efficient meshing grid which is then analyzed according to the calculated tunneling solution, and is adapted to give the best contrast and resolution for the final image. A major improvement with this approach is to substantially reduce the number of grid points needed to reveal high resolution STM images. Although the proposed technique has been developed for contour or height recognition of molecular objects in STM, algorithms are sufficiently robust to provide adequate results in various spectroscopic or microscopic imaging techniques.

Acknowledgments

This work was supported by the Natural Sciences and Engineering Research Council of Canada (NSERC). We are grateful to Julien Dompierre for stimulating discussions.

References

[1] P. Sautet, C. Joachim, Calculation of the benzene on rhodium STM images, Chem. Phys. Lett. 185 (1991) 23–30.
[2] J. Cerdá, A. Yoon, M.A. Van Hove, P. Sautet, M. Salmeron, G.A. Somorjai, Efficient method for the simulation of STM images. II. Application to clean Rh(1 1 1) and Rh(1 1 1) + $c(4 \times 2)$-2S, Phys. Rev. B 56 (24) (1997) 15900–15918.
[3] Y. Yang, M.N. Wernick, J.G. Brankov, A fast approach for accurate content-adaptive mesh generation, IEEE Trans. Image Process. 12 (8) (2003) 866–881.
[4] P.J. Frey, P.L. George, Mesh Generation, Application to Finite Elements, Hermes Science Publishing, 2000.
[5] S. Laflamme, J. Dompierre, F. Guibault, R. Roy, Applying ParMetis to structured remeshing for industrial CFD applications, Int. J. High Perform. Comput. Appl. 17 (1) (2003) 63–76.
[6] C. Manole, M.-G. Vallet, J. Dompierre, F. Guibault, Benchmarking second order derivatives recovery of a piecewise linear scalar field, in: Proceedings of the 17th IMACS World Congress Scientific Computation, Applied Mathematics and Simulation, 2005.
[7] S. Datta, Electronic Transport in Mesoscopic Systems, Cambridge University Press, 2003.
[8] M. Büttiker, Y. Imry, R. Landauer, S. Pinhas, Generalized many-channel conductance formula with application to small rings, Phys. Rev. B 31 (10) (1985) 6207–6215.
[9] J. Cerdá, M.A. Van Hove, P. Sautet, M. Salmeron, Efficient method for the simulation of STM images. I. Generalized Green-function formalism, Phys. Rev. B 56 (24) (1997) 15885–15899.
[10] F. García-Moliner, V.R. Velasco, Theory of a Single and Multiple Interface, World Scientific Publishing, 1992.
[11] P.S. Weiss, D.M. Eigler, Site dependence of the apparent shape of a molecule in scanning tunneling microscope images: benzene on Pt(1 1 1), Phys. Rev. Lett. 71 (19) (1993) 3139–3142.
[12] P. Sautet, M.-L. Bocquet, Theoretical analysis of the site dependence of the shape of a molecule in STM images, Surf. Sci. 304 (6) (1994) L445–L450.
[13] W. Ho, L.J. Lauhon, Single-molecule chemistry and vibrational spectroscopy: pyridine and benzene on Cu(0 0 1), J. Phys. Chem. A 104 (2000) 2463–2467.
[14] J. Tersoff, D.R. Hamann, Theory of the scanning tunneling microscope, Phys. Rev. Lett. 50 (1983) 1998.
[15] N. Lorente, M.F.G. Hedouin, R.E. Palmer, M. Persson, Chemisorption of benzene and STM dehydrogenation products on Cu(1 0 0), Phys. Rev. B 68 (2003) 155401–155409.
[16] B.L. Rogers, J.G. Shapter, M.J. Ford, Ab initio study of benzene on the Cu(1 1 0) surface and simulation of STM images, Surf. Sci. 548 (2004) 29–40.